



Characterizing the interaction of groundwater with surface water and precipitation in the Mongolian Plateau in China

Yitong Zhang¹ · Jiaqi Chen² · Jiansheng Chen³ · Fenyan Ma⁴ · Jiaheng Yan⁵ · Wang Wang¹

Received: 13 February 2023 / Accepted: 12 July 2023 / Published online: 9 August 2023
© The Author(s), under exclusive licence to International Association of Hydrogeologists 2023

Abstract

Due to the arid climate, groundwater is a vital water resource for ecosystems such as those associated with Dalinor Lake in the Inner Mongolian Plateau, China. This research studied the groundwater circulation mechanisms in Dalinor Lake and surrounding areas and their contribution to surface water, based on remote sensing and environmental isotopes analyses. Using Landsat satellite data, it was found that the lake area of Dalinor Lake decreased by 12% between 1986 and 2021. The shrinkage rate increased from 0.31 km²/year in 1986–2005 to 1.24 km²/year in 2005–2021. The groundwater contribution to the lake is 1.49×10^8 m³/year. Soil profiles and a rainfall simulation test revealed that precipitation infiltration provides limited recharge to groundwater. The groundwater stable isotopic signature ($\delta D = -88.55\%$, $\delta^{18}O = -10.01\%$), which is more depleted than local precipitation ($\delta D = -63.83\%$, $\delta^{18}O = -8.76\%$), implies that local precipitation is not the main source of groundwater recharge. The groundwater stable isotopic signature in different river sources is diverse, indicating the spatial specificity of groundwater recharge sources. Groundwater and river water have mantle-derived helium ($R/R_a > 1$) and high tritium concentrations, so it is speculated that groundwater in the Dalinor Lake and its surrounding area is recharged by modern precipitation (post 1960s) outside the study area through fast channels, such as fault systems. This study provides information necessary for effective water management in the Inner Mongolian Plateau.

Keywords Groundwater recharge · Isotopes · Remote and satellite sensing · China

Introduction

The combined pressure of climate drought and human activities has posed a serious challenge to global water resources. Shrinking lakes, degraded wetlands, depleted rivers, and declining groundwater storage have created a crisis for human production and ecosystem maintenance. The Inner Mongolia

Plateau is part of the arid and semi-arid region of China and is located in the southern part of the Mongolian Plateau. The Inner Mongolia Plateau has the most severe shrinkage of lake area in China. As of 2015, the shrinking area of lakes in the Inner Mongolia Plateau reached 22% of the lakes area as compared to the 1960s. The wetland area of the Inner Mongolia Plateau has also lost 8% during two decades (1993~2013), gradually converting to nonwetland types such as arable land (Zheng et al. 2019). The Xiliao River in the eastern part of the Inner Mongolia Plateau has dried up several times in the past decades (Yang et al. 2009). Due to the arid climate and scarce precipitation, the Inner Mongolia Plateau region relies heavily on groundwater resources (Guo et al. 2019; Ma et al. 2022; Wu et al. 2016). However, recent studies show that groundwater storage in eastern Inner Mongolia has shown a decreasing trend (Yin et al. 2021; Zhao et al. 2016). The decline of groundwater level and storage would directly cause the decline of surface-water resources and increase the risk of environmental degradation (e.g., vegetation degradation and land desertification; Li D et al. 2021; Shen et al. 2021a, b).

In the eastern part of the Inner Mongolian Plateau, Dalinor Lake is situated at the west end of the Greater

✉ Jiaqi Chen
jiaqichen@hhu.edu.cn

¹ Geotechnical Research Institute, College of Civil and Transportation, Hohai University, Nanjing 210098, China

² School of Computer and Information, Hohai University, Nanjing 211100, China

³ Water Science Research Institute, Hohai University, Nanjing 210098, China

⁴ College of Energy and Power Engineering, Lanzhou University of Technology, Lanzhou 730000, China

⁵ Faculty of Architecture and Civil Engineering, Huaiyin Institute of Technology, Huaian 223003, China

Khingyan Mountains and the north side of the Yinshan Mountains. As an important national nature reserve in the Inner Mongolia Plateau, the area is rich in water resources that support human life in the surrounding area and provide a habitat for many rare bird species (SEPA 2001). The Dalinor Lake area has gradually declined in recent years, including lake area shrinkage and depleted rivers. The Xilamulun and Laoha rivers to the east of the surrounding area of Dalinor Lake are the two sources of the Xiliao River, whose downstream basin is an important grain-producing area in China. However, in recent decades, the Xiliao River has dried up several times due to unreasonable water allocation and climate drought (Yang et al. 2009). Dalinor Lake has shrunk significantly under the combined influence of human activities and climate change, and the salinity of the lake is gradually increasing (Bai et al. 2020; Xing et al. 2021; Xu et al. 2022). A sharp drop in groundwater level occurred in the sands of the Hunsandak region west of Dalinor Lake at approximately 4.2 cal ka BP (thousand calibrated years Before Present), causing shrinkage of the ancient Dalinor Lake and down-cutting of the Xilamulun River course (Yang et al. 2015). Although the precipitation in Dalinor Lake area has increased since ca. 1.3 cal ka BP, the lake level has shown the opposite trend (Zhen et al. 2021). These phenomena display the role of groundwater in controlling surface-water resources in the region. The shrinkage of Dalinor Lake and the depletion of the Xiliao River are the epitomai of water resource loss in the Inner Mongolia Plateau. Exploring the groundwater circulation mechanism in this region can provide a reference for water resources management in Inner Mongolia Plateau and even in arid and semiarid regions.

Recharge is a crucial component of the overall groundwater circulation mechanism. Due to the complexity of recharge processes, groundwater recharge relationships in the Inner Mongolia Plateau region are not completely understood. Zhu et al. (2019) found no seasonality in the groundwater stable isotope composition and concluded, by hydrogen-oxygen stable isotope analysis, that local precipitation is not the main source of groundwater recharge in Dalinor Lake region. And Zhu et al. (2019) determined, with analysis by the same means, that the groundwater in the Hunsandak region, which is next to Dalinor Lake, recharges from precipitation in the eastern mountains. Hydrogen and oxygen stable isotopes are the most common means of exploring interactions among water bodies, and stable isotopes of atmospheric precipitation are the basis for using this method. The current lack of long-term monitoring of hydrogen and oxygen isotopes in precipitation near Dalinor Lake affects the accuracy of the results of the analysis of interactions between the water bodies by isotopic means.

The main objectives of this research are: (1) to determine the contribution of groundwater to Dalinor Lake; and (2) to identify the relationship between the groundwater and other natural water bodies in Dalinor Lake basin and surrounding area and the groundwater circulation mechanisms. Remote sensing, unsaturated-zone soil profiles and environmental isotopes analyses of water bodies in the study area were used to achieve the objectives of this study. In addition, a long-term precipitation stable isotope monitoring meteorological film, established in the city of Erenhot, was used to address the lack of long-term precipitation isotope monitoring in the study area. The results of this study will help to provide a reference for water resource management in the Inner Mongolia Plateau.

Study area

Dalinor Lake (Fig. 1c; 43°13′~43°23′ N, 116°26′~116°45′ E) is located in the western part of the Inner Mongolia Plateau, west of the southern end of the Greater Khingyan Mountains, north of the Hunsandak Sands, and surrounded by a basalt plateau formed by the Cenozoic eruption to the northwest (Fig. 1b). Dalinor Lake is about 21 km from north to south and 15 km from east to west, with a water storage capacity of about $16 \times 10^8 \text{ m}^3$ and a lake elevation of 1,226–1,228 m above sea level, shallow in the east and deep in the west, with an average depth of 6.7 m and a maximum depth of 13 m (Xing et al. 2021). Dalinor Lake is located at the northern edge of the East Asian summer winds, with a temperate continental monsoon climate, an annual average temperature of 1–2 °C, and annual precipitation between 140 and 509 mm. The annual potential incremental evaporation can be up to 2,000 mm, much larger than the annual precipitation.

Dalinor Lake is an endorheic lake that is recharged by groundwater, rivers, and local precipitation, and is discharged only by evaporation. Four rivers recharge Dalinor Lake, namely the Gunger, Liangzi, Shali, and Haoli rivers, all of which have springs as their sources (Zhen et al. 2014). In addition, Dalinor Lake also receives direct recharge from groundwater, including the Dashui and Xiaoshui springs under the Mantuo Mountain on the south shore.

The study area (Fig. 1b) is located between the North China Craton (NCC) and the Central Asian Orogenic Belt (CAOB; Fig. 1a). Extensive fissure and fault networks prevail, and the Solonker suture crosses the area. In addition, two major EW strike faults cross the study area—the Chifeng-Baiyan Obo Fault and the Xar Moron fault (Zhang et al. 2014; Fig. 1b). The Xar Moron fault is an ultra-crust fault formed in the Late Permian and Early Triassic, and the fault changed from compressional to tensional after the Quaternary. On the other hand, the Chifeng-Baiyan Obo Fault is the dividing line between the NCC and the CAOB. The

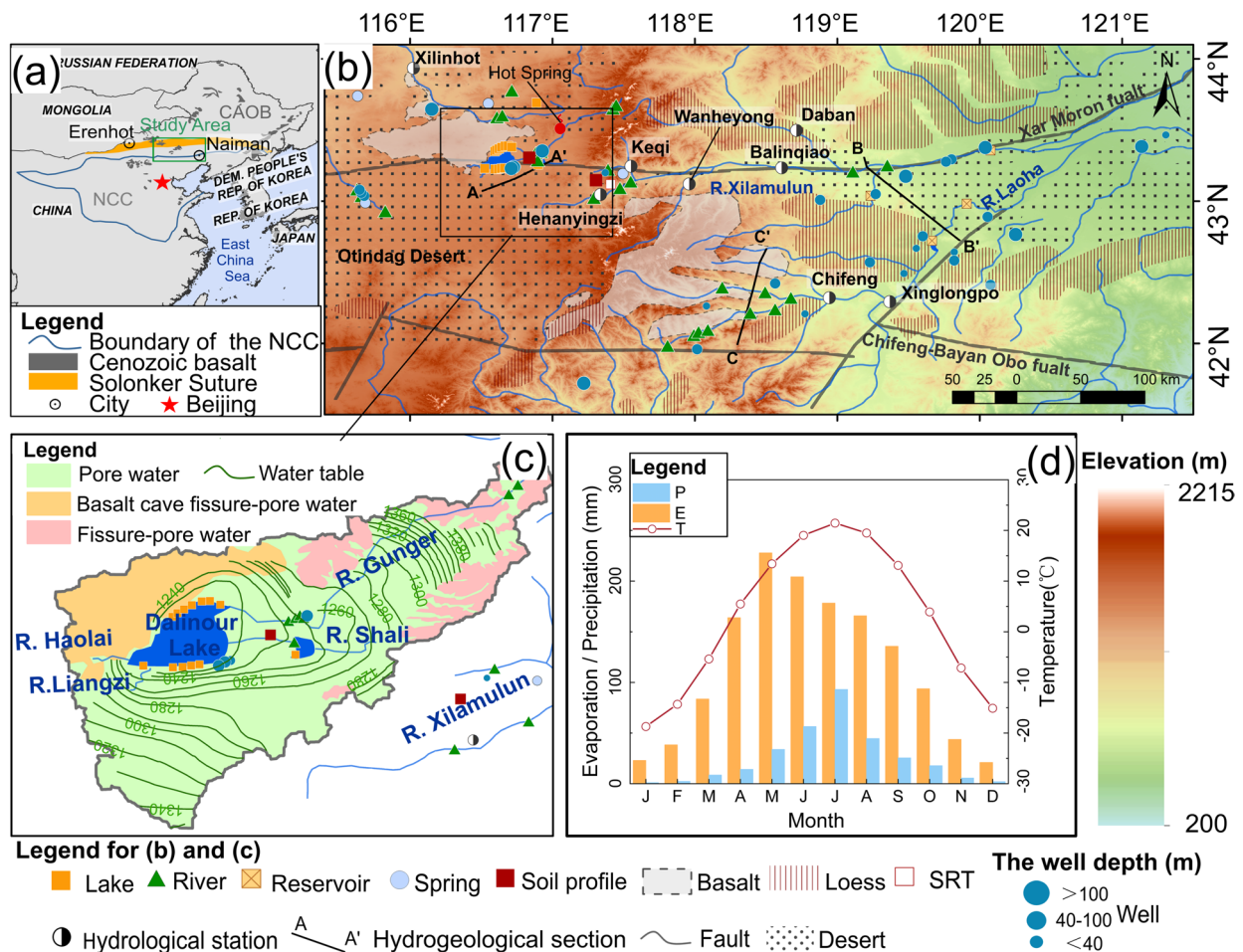


Fig. 1 a Geotectonic setting of the study area. NCC North China Craton, CAOB Central Asian Orogenic Belt. Image modified from Gong et al. (2016), Huang et al. (2019), Ye et al. (2020) and Zhang et al. (2014). b Details of the study area and sampling points. SRT stands for simulated rainfall test; image adapted from Ye et al. (2020). The

hydrogeological sections in the figure are adapted from Mu et al. (2021). Refer to Table S1 of the electronic supplementary material (ESM) for the specific depth of well samples. c The Dalinor Lake basin image is adapted from Li W et al. (2021). d evapotranspiration (E), precipitation (P) and air temperature (T) data for the study area

topographic and geomorphic formation in the study area is closely related to the neotectonic movement. Dalinor Lake was formed by tectonic subsidence and basaltic lava flows (Li W et al. 2021; Ye et al. 2020). Cenozoic basaltic rocks are widely exposed in and around Dalinor Lake such as the Dalinor basalt near Dalinor Lake and the Hanoba basalt located in the Chifeng area (Gong et al. 2016). Quaternary sediments are the main aquifers in the study area. Around the lakes and in the middle and lower reaches of the rivers, groundwater is stored as pore water in the quaternary unconsolidated rocks aquifers which can be more than 200 m thick—Figs. S1 and S2 of the electronic supplementary material (ESM). In the mountains, groundwater is mainly in the form of bedrock fissure water and clastic rock pore-fissure water in aquifers composed of magmatic rocks such as tuffaceous sandstone, basalt and andesite, and sedimentary rocks such as sandstone. In addition, in the river valley

area, aquifers composed of Quaternary sediments less than 40 m thick are present (Fig. S3 of the ESM).

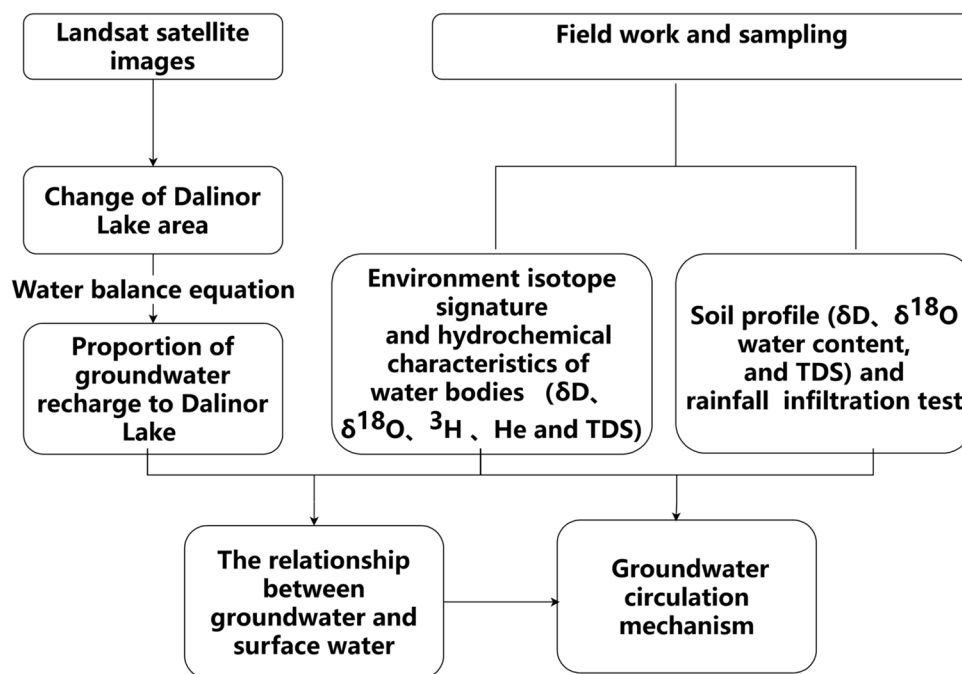
Materials and methods

The flow chart (Fig. 2) briefly explains the work done in this study and the logic of the research.

Remote sensing data

Landsat series satellite data are widely used for surface changes (Dong et al. 2020; Pekel et al. 2016; Zheng et al. 2016). In this study, the Landsat satellite images from 1986 to 2021 were selected to extract the area of Dalinor Lake. The data were obtained from the United States Geological Survey website (USGS 2011) and the Geospatial Data Cloud site, Computer

Fig. 2 Flow chart for the components of this study



Network Information Center, Chinese Academy of Sciences website (CAS 2015). Since weather conditions such as clouds can significantly affect the quality of satellite images by blurring the lake boundaries, images from July and August were selected when the proportion of cloud cover was low. Images from adjacent months were interpolated when no images were available. ENVI 5.3 software was used to reconstruct the satellite images to improve the clarity of remote sensing images. The cumulative anomaly analysis is a method commonly used in climate change research to study abrupt changes in time series (Lozowski et al. 1989; Qin et al. 2019; Wang et al. 2017a). In this study it was used to identify the characteristics of lake area changes over time. To study the groundwater circulation, hydrological and meteorological data were collected from the Hydrological Yearbooks (2006–2011).

The groundwater discharge of the Dalinor Lake is calculated according to the water balance equation (Eq. 1) (Ma et al. 2022):

$$Q_G = \Delta Q - A \times P - Q_R + A \times E \quad (1)$$

where A is the area of the Dalinor Lake, km^2 , ΔQ represents the change in lake storage in the Dalinor Lake, m^3/year ; Q_R is the sum of the annual river inflows to the Dalinor Lake, m^3/year ; P and E are the precipitation and evaporation (mm) of the Dalinor Lake, respectively, and Q_G is the groundwater discharge to the Dalinor Lake, m^3/year . P , E , and Q_R data are measured at hydrological stations (Xing et al. 2021). The surface evaporation E can be obtained by multiplying the measured data from the $\phi 20$ evaporation pan by a conversion factor, which is 0.6 according to previous studies (Bai et al. 2020).

Water sampling

The natural water samples were collected in July 2013. A total of 81 water samples were collected, including well water (31), spring water (4), river water (28), lake water (14), and reservoir water (4). The locations of the sampling sites are shown in Fig. 1b. Water samples were analyzed using a multi-parametric analyzer (Multi 3400i, WTW, Germany) to measure the pH and total dissolved solids (TDS) values with an analytical error of <10%. The collected water samples were stored in high-density polyethylene bottles sealed with tape to prevent isotopic fractionation. The water samples for the determination of helium isotopes were collected in specialized sodium glass bottles, which have low He-permeability characteristics. When taking a water sample, the operator opened the valves at both ends simultaneously and allowed the water to slowly enter the glass bottle. The valves were closed when the bottle was completely full and free of air bubbles, and the valves were taped tightly to prevent air contamination during transport and storage. All samples were measured within 2 weeks of collection. The samples were sent to the State Key Laboratory of Hydrology, Water Resources, and Hydraulic Engineering, Hohai University (China), for isotope analysis. Precipitation in the city of Erenhot was collected between 2015 and 2019, and data on precipitation in Naiman were obtained from the Chinese Network of Isotopes in Precipitation (CHNIP; Liu et al. 2014).

Hydrogen and oxygen stable isotope compositions were determined using a MAT253 mass spectrometer (Thermo Fisher Finnigan, Waltham, Massachusetts, USA). The

analytical precisions for $\delta^2\text{H}$ and $\delta^{18}\text{O}$ were ± 2 and $\pm 0.1\%$, respectively. The hydrogen and oxygen stable isotope data are expressed as parts per thousand relative to Vienna Standard Mean Ocean Water (VSMO) using the delta (δ) notation. A liquid scintillation meter (TRI-CARB 3170 TR/SL) was used to measure the tritium concentration in samples. It has a detection limit of 0.2 TU and analytical precision of >0.8 TU. Isotopic signatures of helium and neon were measured using a VG5400 static mass spectrometer. The precision of the measurements was >0.6 and $>2.5\%$ for $^3\text{He}/^4\text{He}$ and $^4\text{He}/^{20}\text{Ne}$ values, respectively.

Helium in groundwater consists of three sources—the atmosphere, the mantle, and the crust. Since the $^3\text{He}/^4\text{He}$ ratio in different sources varies, the contribution of each helium source to helium in groundwater is judged by the $^3\text{He}/^4\text{He}$ ratio. The $^3\text{He}/^4\text{He}$ (R_a) ratio in the atmosphere is considered constant (1.4×10^{-6} ; Marty and Le Cloarec 1992). Assuming that all the neon in the samples is derived from atmospheric derivatives, the helium isotope ratios in samples that are air-contaminated can be corrected by measuring the $^4\text{He}/^{20}\text{Ne}$ ratios in the samples (Hilton 1996):

$$R_c/R_a = (R_m/R_a \times X - 1)/(X - 1) \quad (2)$$

where R_c/R_a represents the air-contaminated corrected helium isotopic ratio ($R_a = 1.4 \times 10^{-6}$) (Marty and Le Cloarec 1992); R_m/R_a represents the measured helium isotopic ratio. X is the air-normalized $^4\text{He}/^{20}\text{Ne}$ ratio. $X = (^4\text{He}/^{20}\text{Ne})_{\text{measured}} / (^4\text{He}/^{20}\text{Ne})_{\text{air}} \times (\beta_{\text{Ne}}/\beta_{\text{He}})$, where $(^4\text{He}/^{20}\text{Ne})_{\text{measured}}$ and $(^4\text{He}/^{20}\text{Ne})_{\text{air}}$ are the $^4\text{He}/^{20}\text{Ne}$ ratios of measured samples and air (0.3185), respectively. (Ozima and Podosek 2002), β_{Ne} and β_{He} are the Bunsen solubility coefficients for Ne and He, respectively, from WEISS (1971), assuming the temperature of the water sample is 20 °C.

The proportion of mantle-derived helium in the sample was calculated from the air-corrected helium isotope ratio (Hilton 1996):

$$\text{PM} = (R_m - 0.002R_a)/(8R_a - 0.002R_a) \quad (3)$$

where PM is the proportion of mantle-derived helium in the sample; $8R_a$ and $0.002R_a$ are the $^3\text{He}/^4\text{He}$ ratio of mantle and crust, respectively (Ballentine and Burnard 2002; Graham 2002). The results are shown in Table S1 in the ESM.

In July 2013, soil profiles were collected around Lake Dalinor and a simulated rainfall test was conducted (Fig. 1b and Table S2 in the ESM). The depths of profiles A and B were 315 and 310 cm, respectively. The soil profiles were sampled at 20-cm intervals. A rainfall simulation test was carried out on a flat sand layer. A shallow square pit with sides of 100 cm \times 100 cm \times 2 cm was dug at the test site. A total of 400 L of water ($\delta\text{D} = -83.7\%$, $\delta^{18}\text{O} = -10.6\%$) was injected into the shallow pit and allowed to infiltrate by gravity. Considering previous precipitation infiltration

research in the desert, heavy precipitation has little effect on moisture content of soil below 40 cm depth, even after 182 h (Wang et al. 2003). And local precipitation events >20 mm occur less than 3 times a year (Ren et al. 2018). Therefore, a soil profile was excavated in the center of the square column after 48 h of water injection, and soil samples were collected at a depth interval of 20 cm. Since the water was not in full vertical motion during infiltration, the impact of the injected water was found to be 160 cm \times 160 cm \times 100 cm after excavation. The simulated rainfall was 156 mm, which was much greater than the single maximum precipitation event in the study area. To compare with the simulated rainfall profile, test-site soil samples were taken from the natural profile at 5 m with the same sampling interval and depth as the simulated rainfall profile. Soil samples were sealed and sent to the laboratory for testing. Gravimetric water content was determined by an oven-drying method with an analytical precision of better than 1% (Shurbaji et al. 1995). Soil water was extracted from soil samples using vacuum distillation to analyze δD and $\delta^{18}\text{O}$ content, which was carried out using a MAT253 mass spectrometer. To analyze TDS in soil water, 100 g of air-dried soil (air dried for 48 h) were mixed with 100 ml of deionized water. The mixture was equilibrated for 48 h, during which time it was stirred periodically. The leachate was filtered through a medium-speed quantitative filter paper for TDS measurement after equilibration. The TDS values in the leachate were converted to values in soil water using the following formula.

$$\text{TDS}_s = \frac{\text{TDS}_l \times V_w \times \rho_w}{m_s \times w} \quad (4)$$

where TDS_s is the TDS value in the soil water, mg/L; TDS_l is the TDS value in the leachate, mg/L; V_w is the volume of deionized water; m_s is the mass of air-dried soil, mg; w is the gravimetric water content; ρ_w is the density of water, mg/L.

Results

The change of Dalinor Lake area

The annual time series of the lake area of Dalinor Lake extracted from Landsat satellite images is shown in Fig. 3. Overall, the lake area decreased from 211.4 km² (1986) to 185.6 km² (2021), a decrease of 12% with a significant downward trend of $p < 0.01$ (p indicates significance level). The cumulative anomaly of the lake area increases from 2005 and decreases after 2005. Combined with the cumulative anomaly analysis (Fig. 3), the lake area changed in two phases: (1) from years 1986 to 2005, the lake area shrank by 2.8% at a rate of -0.31 km²/year ($p < 0.05$); (2) from

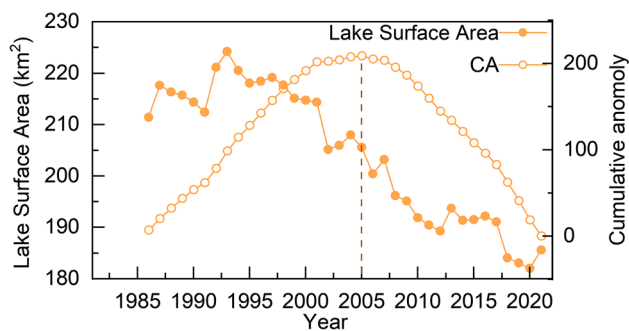


Fig. 3 Interannual variation of the Dalinor Lake area and trends in the cumulative anomaly (CA) of the lake area

years 2005 to 2021 the lake area decreased by 9.7% significantly ($p < 0.001$) at a rate of $-1.24 \text{ km}^2/\text{year}$. The lake area underwent an abrupt change in 2005 (the rate of lake area loss increased).

Distribution of stable isotopes, water content, and TDS in the unsaturated zone

As a bridge between groundwater and precipitation, study of soil water is crucial for exploring groundwater circulation mechanisms, especially in arid and semiarid regions (Li et al. 2017). Samples from soil profiles were collected at the Dalinor Lake basin and the source of the Xilamulun River, respectively (Fig. 1b). The distributions of gravimetric water content, TDS, δD , and $\delta^{18}\text{O}$ for profile A (sand with clay particles) and profile B (sand) are shown in Fig. 4.

The TDS and stable isotopes curves of soil water show an opposite trend to the water content, indicating that soil moisture is affected by soil evaporation. Figure 4a, b shows that δD , $\delta^{18}\text{O}$, and TDS values in profile A show an overall decreasing trend with increasing profile depth. Soil water

δD below 100 cm is more depleted than precipitation δD . If precipitation recharges both deep soil water and groundwater, these substances will mix with the next precipitation and infiltrate with it into deep soil water and groundwater. Therefore, the TDS of soil water should increase with depth, which indicates that precipitation cannot recharge the deep soil water. Under the influence of evaporation, various substances will accumulate in the soil near the surface.

Fluctuations of the TDS content and the stable isotope signature are more pronounced in profile B, which is attributed to evaporation–condensation processes and the soil properties. Compared to profile B, the soil moisture in profile A is higher for the site near the river. Composed primarily of sand, Profile B presents an even soil grain-size distribution throughout its depth. Profile B has a soil-moisture deficit comparable to the maximum field capacity (5%) that is typical of sandy soils. During precipitation infiltration, the soil-water content must reach the maximum field capacity before the water can infiltrate further. When the water content is below this value, the hydraulic conductivity is very low, so the water redistribution process caused by the hydraulic gradient in soil can be neglected (Gardner 1960). Based on this, a rough estimation suggests that precipitation infiltration, excluding evaporation, can recharge deep soil water to a depth of 320 cm with a single rainfall event of 130 mm. This volume is nearly half of the annual precipitation in the study area. It can be assumed that precipitation struggles to effectively recharge deep soil water and groundwater by piston flow.

A simulated rainfall test was conducted near profile B, aiming to determine the potential of precipitation infiltration in recharging the groundwater. The curves of soil gravimetric water content, TDS, δD , and $\delta^{18}\text{O}$ with depth before and after the simulated rainfall experiment are shown in Fig. 5. The soil gravimetric water content of the natural

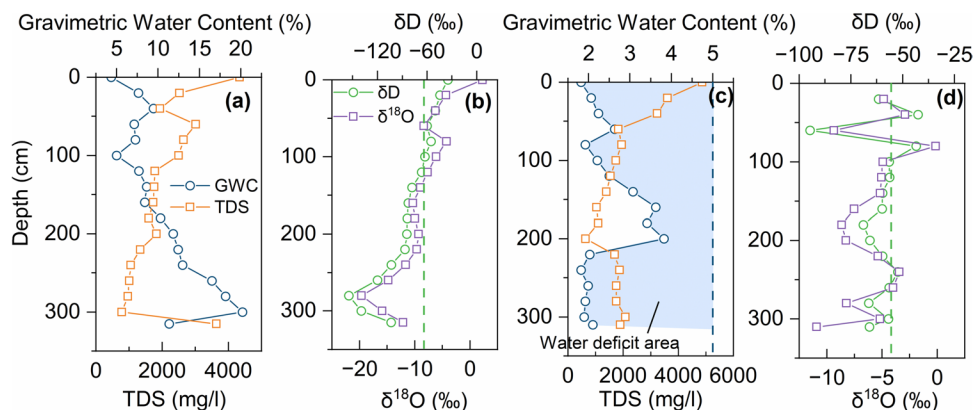
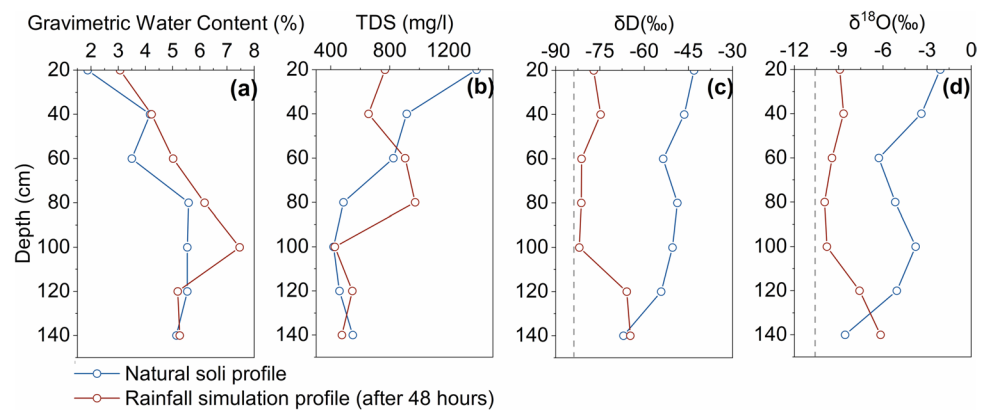


Fig. 4 Distributions of δD , $\delta^{18}\text{O}$, gravimetric water content, and TDS in soil profiles: **a–b** represents profile A; **c–d** represents profile B. The dashed line represents the annual weighted average of precipitation hydrogen isotopes ($\delta\text{D} = -63.83\text{‰}$) (**b** and **d**). **c** Dashed line

represents the maximum field capacity (MFC) of the sandy soil with a value of 5% (Goldberg et al. 1976), and the blue shading indicates the soil-water deficit areas, indicating a soil-moisture content below the MFC

Fig. 5 The gravimetric water content (a), TDS (b), δD (c), and $\delta^{18}O$ (d) with depth in the simulated rainfall profile and natural profile. c and d Dashed lines represent the precipitation hydrogen and oxygen stable isotope compositions used for simulation ($\delta D = -83.7\text{‰}$, $\delta^{18}O = -10.56\text{‰}$)



profile increases with depth at the 0–80 cm stage and stabilized in the area below 80 cm (average 5.35%). The TDS curve shows an inverse trend when compared to the soil-moisture curve. The TDS profile stabilizes below 100 cm (average 468 mg/L) and converges towards groundwater TDS (420 mg/L). Meanwhile, the stable isotope profiles exhibit S-shaped changes with increasing depth under the synergistic effects of precipitation infiltration and evaporation condensation. After the 48-h period of the simulated rainfall test, the soil-moisture profile increases with depth over 100 cm and approaches the natural profile at 120 cm. The stable isotopes gradually align with the initial soil-water isotopic signature and the soil-water TDS content is similar to the natural profile below 100 cm depth. The simulated rainfall test showed that 156 mm of rainfall cannot affect the unsaturated zone at a depth greater than 100 cm, so it was difficult for precipitation to recharge groundwater.

Isotopic signature in different water bodies

When using the hydrogen-oxygen isotope method of analysis, it is crucial to compare the isotope signatures of the water samples to the local meteoric water line (LMWL). Establishing the LMWL requires long-term precipitation isotope monitoring data. Owing to the absence of multi-year continuous hydrogen-oxygen stable isotope monitoring of precipitation in the study area, previous research often utilized data from the Tianjin and Baotou stations supplied by the Global Network of Isotopes in Precipitation (GNIP) network, or collected single precipitation samples (Li et al. 2019; Zhu et al. 2019). However, there is significant elevation difference between Tianjin (2 m asl) and the study area, and the Baotou station is located in the interior of the continent; therefore, these two sites experience very different altitude effects, latitudinal effects and continental effects compared to the study area. Hence, precipitation isotope data from Erenhot (Fig. 1a) located on the Inner Mongolia Plateau and unseparated from Dalinor Lake by mountains, possessing similar latitude

and elevation for the study area, was selected instead of the study area. Precipitation isotope data from Naiman, situated west of the study area and closer to the sea (Fig. 1a), was also incorporated (Liu et al. 2014), aiming at a more comprehensive set of data on precipitation isotopes within the study area.

Hydrogen-oxygen stable isotopic signature data were collected for precipitation for five consecutive years from 2015 to 2019. Of the total weighted average of all isotope data weighted by precipitation amount, the summer data have the largest footprint, as the precipitation from June to August accounts for 56% of the annual precipitation. The precipitation hydrogen-oxygen stable isotopic signature is enriched in summer and depleted in winter. This isotopic signature aligns with that of precipitation in other regions situated on the Inner Mongolia Plateau (Liu et al. 2014). The weighted average values of δD and $\delta^{18}O$ of monthly precipitation are -63.83 and -8.76‰ , respectively. The comparison indicates that the precipitation isotopes in Naiman align closely with the weighted average of the precipitation isotopes in Erenhot, suggesting that the use of precipitation isotopes in Erenhot as representative of the study area's precipitation characteristics is justified. The monthly weighted average of precipitation δD – $\delta^{18}O$ was computed based on five consecutive years (2015–2019) of observed data to obtain the LMWL, which is similar to the LMWL obtained by previous researchers for Dalinor Lake in summer ($\delta D = 8.22\delta^{18}O + 6.82$; Li et al. 2019). Compared with the global meteoric water Line (GMWL) ($\delta D = 8.00\delta^{18}O + 10$), the slope and intercept of LMWL are relatively small, which is associated with subcloud evaporation during precipitation. This is a common phenomenon in arid and semiarid regions (Dogramaci et al. 2012; Zhang and Wang 2016).

In order to delve deeper into the features of groundwater recharge and discharge, natural water samples were collected for isotopic analysis in and surrounding the Dalinor basin, including the source of the Xiliao River. The δD , $\delta^{18}O$, TDS, and pH values of the lake water, river water, well water, spring water, and reservoir water in the Dalinor basin and

its surrounding areas are depicted in Fig. 6 (more details in Table S1 of the ESM). Well water and springs have similar isotopic signatures, representing groundwater samples. Surface water shows wide isotopic distribution with δD and $\delta^{18}O$ values of -29.50 to -80.30‰ and -1.03 to -15.77‰ , respectively. Additionally, river samples were mainly collected at the source of the river, and fieldwork and previous studies have shown that most rivers originate from springs (Li W et al. 2021; Yang et al. 2015; Yu et al. 2020). River samples from the source are influenced by groundwater. Consequently, river samples share isotopic and hydrochemical characteristics with groundwater.

Given its short half-life, tritium is often utilized to probe the age of groundwater circulation. Tritium concentrations were determined for samples from rivers, wells and springs in the study area (Table S1 in the ESM). The tritium concentration was detected in three river water samples (R7\R8\R10) and the average value was 17.05 TU; the average value of tritium concentration of groundwater samples (W5\W6\W9) was 91.56 TU. Excluding the higher value of sample W6, the mean value becomes 17.11 TU, which is close to the tritium concentration in river water. The tritium value for W6 decreased to 40 TU after 3 months. There exist differences in tritium concentrations among groundwater samples, which are related to the rate of groundwater circulation. China conducted extensive nuclear testing in its northwestern atmosphere in the 1960s and 1980s, resulting in a significant increase in tritium in precipitation in nearby areas (Ren et al. 2005). Tritium infiltrates groundwater with precipitation during the process of groundwater recharge. Tritium concentrations in groundwater, recharged by precipitation, display variability but are generally higher than in other areas due to distinct runoff pathways and circulation times. Moreover, tritium in groundwater on the Inner Mongolian

Plateau has been observed to exhibit high background values in investigations since 2000 (Ren et al. 2005). Groundwater runoff is thought to resemble a piston movement; hence, the high tritium precipitation following nuclear testing can induce spikes in tritium in groundwater runoff.

The $^3\text{He}/^4\text{He}$ ratio (R) is frequently used to trace groundwater circulation (Mahara and Lgarashi 2003; Stute et al. 1992). Groundwater and river water samples were gathered along the fracture zone to ascertain whether groundwater circulation was influenced by geological formations. The $^3\text{He}/^4\text{He}$ ratios in the sampled well water, spring water, and river water are displayed in Table S1 of the ESM. The R_m/R_a values of well and river samples are all >1 . Three of the spring samples exhibited R_m/R_a less than 1, while one sample had a value greater than 1. Overall, the results indicate a correlation between groundwater circulation and geological formations.

Discussion

The contribution of groundwater to Dalinor Lake

Dalinor Lake is an endorheic lake, and evaporation constitutes the sole discharge mechanism for the lake. Because the lake water level is lower than the groundwater level (Fig. 1c), Dalinor Lake receives groundwater recharge in addition to precipitation and river water. The contribution of groundwater to the lake is quantified using a water balance equation (Eq. 1), as explained in section 3.3.1. The change in lake storage (ΔQ) in the equation is calculated based on the lake area (A). According to the equations of water storage (Q)-depth (D) and area (A)-depth (D) relationships monitored by Xing et al. (2021), the relationship

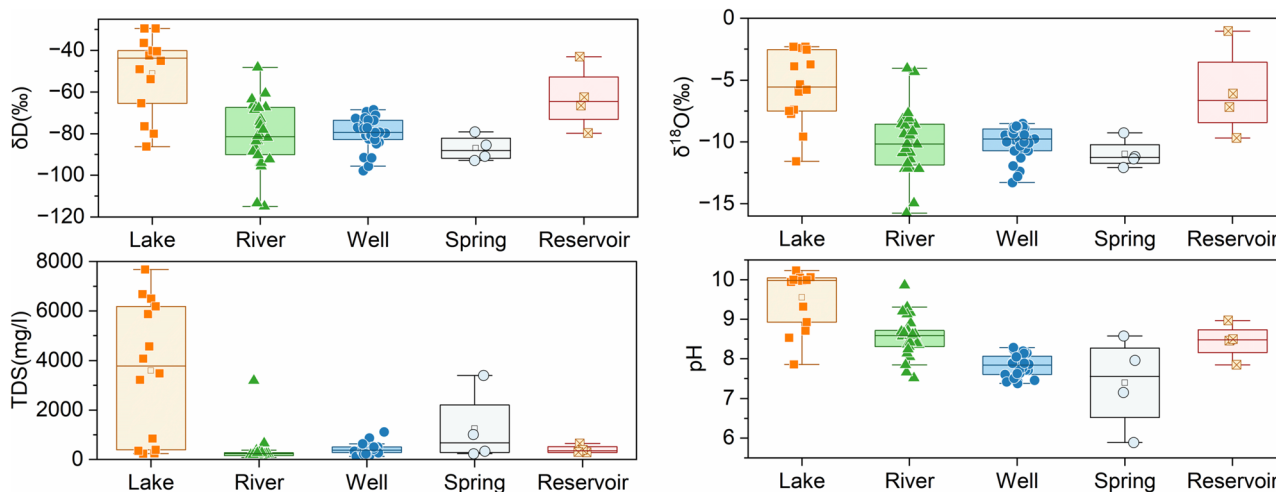


Fig. 6 Isotopic and hydrochemical characteristics of groundwater and surface water

between water storage (Q) and area (A) was obtained with fitting to get a nonlinear model: $Q = 0.9405 + 37881A - 0.00435A^2 + 2.12564 \times 10^{-5}A^3 - 3.51188 \times 10^{-8}A^4$ ($R^2 = 0.98$). The calculation results are presented in Table S3 of the ESM. The results indicated that the groundwater discharge range of Dalinor Lake from 2008 to 2017 was between 1.14×10^8 and $2.03 \times 10^8 \text{ m}^3$, with a mean discharge value of $1.49 \times 10^8 \text{ m}^3$ and groundwater discharge accounting for 62.5% of the annual recharge of the lake (Fig. 7). Groundwater discharge plays a significant role as a source of recharge to Dalinor Lake.

The recharge of groundwater exhibits an increasing trend over time (Fig. 7). The groundwater storage in the study area has been declining (Yin et al. 2021). Generally, the decrease in groundwater storage should lead to a reduction in groundwater contribution to surface water. However, this process often exhibits a lagged response. By analyzing the second-order difference of groundwater discharge (i.e., the change in groundwater discharge), it is observed that the change in groundwater discharge shows a decreasing trend. This indicates that although the groundwater recharge is increasing, this upward trend will gradually slow down over time. It can be predicted that in the future, this upward trend will cease and then decline along with the decrease in groundwater storage.

Relationship between groundwater and surface water

From a water balance perspective, groundwater constitutes 62.5% of the recharge sources in Dalinor Lake. The groundwater is critical to Dalinor Lake. A comparison of runoff depths of rivers around Dalinor Lake (Table S4 in the ESM) indicates a lack of correlation between runoff depth and precipitation in each basin. For example, despite stations Keqi and Henanyingzi being in proximity (Fig. 1b), their runoff

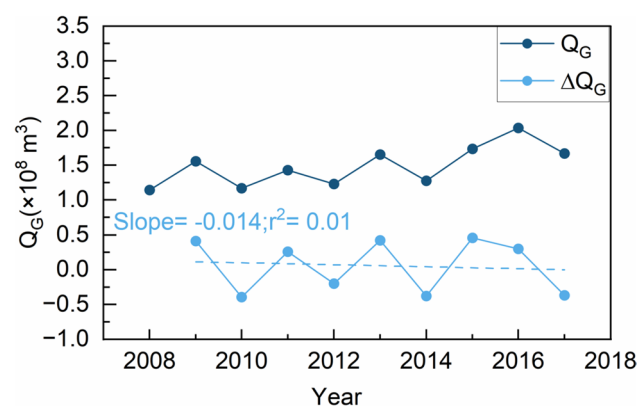


Fig. 7 Interannual trends in groundwater discharge (Q_G) and the amount of variation in groundwater discharge (ΔQ_G)

depths differ by magnitude. Surface water in the region is primarily recharged by both groundwater and precipitation. The significant difference in runoff depth between these basins, despite similar precipitation levels, underscores the crucial role of groundwater in recharging surface water.

From an isotopic perspective, the isotopic characteristics of lake water in different seasons in Dalinor Lake show similarities (Fig. 8b), indicating a stable source of recharge for the lake (Du et al. 2019, Zhen et al. 2014). The evaporation line (EL), derived from the δD and $\delta^{18}O$ relationship of surface-water samples, is depicted in Fig. 8b. The intersection of EL and LMWL can be used to compensate for evaporative effects and determine the isotopic characteristics of surface-water recharge sources (Bowen et al. 2018). If precipitation is the primary recharge source of surface water, then the intersection of the EL and LMWL should approximate the precipitation isotopic signature. The intersection of EL with LMWL ($\delta D = -89.30\text{‰}$, $\delta^{18}O = -11.74\text{‰}$) is significantly lower than the annual weighted average of local precipitation ($\delta D = -63.83\text{‰}$, $\delta^{18}O = -8.76\text{‰}$) and closer to the δD and $\delta^{18}O$ composition of groundwater ($\delta D = -80.55\text{‰}$, $\delta^{18}O = -10.00\text{‰}$) (Fig. 8b). The δD and $\delta^{18}O$ relevant points of L1, L2, L10, and L12 in the lake water samples are closely align with LMWL (Fig. 8b), indicating the influence of precipitation. While the other lake water samples (L3–L9, L11 and L14) and all reservoir water samples are close to EL (Fig. 8b), implying the contribution of groundwater to surface water. Samples collected at the river source indicate that groundwater isotopes are more depleted than river water, suggesting groundwater recharge to the river (Fig. 8c). It is noteworthy that the river water samples are even more depleted in R5 and R6 than the groundwater samples. Field investigations revealed that the river receives spring recharge, which contributes to its depleted isotopes. Overall, groundwater and precipitation both contribute to surface-water recharge, but groundwater is the main source of surface-water recharge (Dai et al. 2014).

The recharge of groundwater

Sand and loess are the main soil types in the study area. The collected soil profiles are all located in sandy areas. The results of the field profiles have indicated that the possibility is low that groundwater is recharged by local precipitation through way of piston flow in the sandy unsaturated zone. Moreover, the particle size of the sand layer is relatively uniform in the study area, that is, the infiltration intensity of the soil is similar. Clay is only found in the section around the lake or near the river, and the stronger water repellency of clay than sand and the existence of vegetation may cause preferential flow (Dekker and Ritsema 1996; Niu et al. 2006). However, for the wider region, the probability of preferential flow is low because the local precipitation

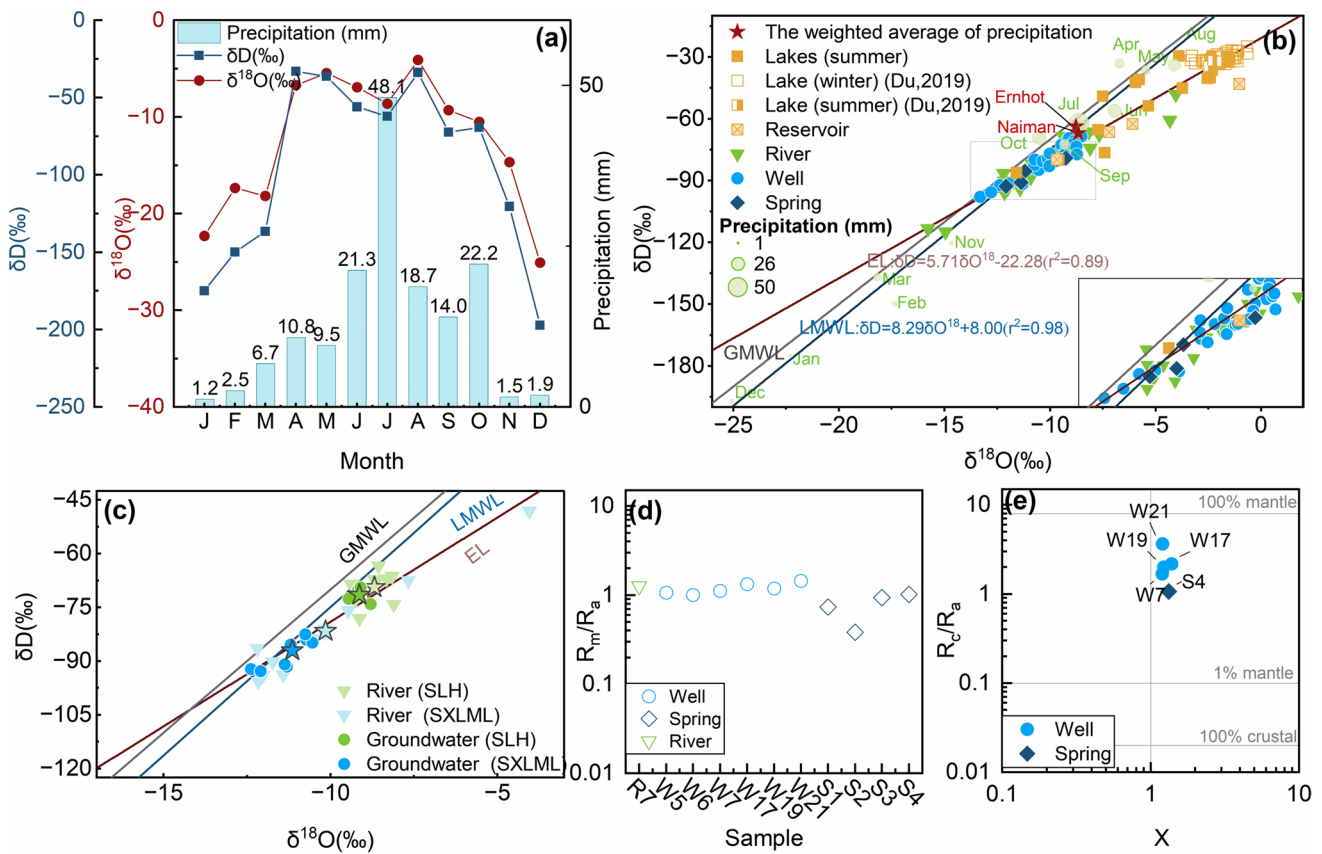


Fig.8 **a** Monthly variation of precipitation amount and isotopes from 2015 to 2019 in Erenhot, which is used in this study to represent the isotopic signature of precipitation in Dalinor Lake and its surrounding basins. **b** Hydrogen and oxygen stable isotope signature of natural waters in the study area; some groundwater data were obtained from Du et al. (2019). **c** Stable isotope compositions of surface water and

groundwater in the sources of the Xilamulun River (SXLML) and the Laoha River (SLH), where the two stars represent the average for the river and groundwater samples separately. **d** Characteristics of uncorrected helium isotope ratios of river water and groundwater. **e** Characteristics of air-corrected helium isotope ratios of river water and groundwater; $X = (^4\text{He}/^{20}\text{Ne})_{\text{measured}} / (^4\text{He}/^{20}\text{Ne})_{\text{air}} \times (\beta_{\text{Ne}}/\beta_{\text{He}})$

intensity is much less than the infiltration rate of the sand layer (Ma et al. 2016; Zhang et al. 2017). Compared to sand, loess has a greater maximum field capacity; therefore, for loess, it is more difficult for precipitation to recharge groundwater effectively through the unsaturated zone within the same precipitation and evaporation conditions. Moreover, the simulated rainfall for loess has shown that it is difficult for groundwater to effectively recharge by precipitation through large pore spaces and vertical joints (Du et al. 1997). Since the evaporation intensity in the study area is more significant than the precipitation intensity, the effect of precipitation on the soil water is mainly concentrated in the top soil layer, with limited contribution to deep soil water and groundwater. This is like the results of previous studies in the Inner Mongolia steppe and the Kubuqi Desert (Ge et al. 2016; Zhang et al. 2020); however, interpretation of the soil profile results is limited due to the heterogeneity of the soils. Isotopic analysis is often employed to study the origins of groundwater, as it is sensitive to processes such as mixed evaporation.

Existing groundwater is formed by the long-term mixing of recharge sources. If groundwater originates from local precipitation, its stable isotopic signature should be more enriched compared to the weighted average of local precipitation. This is because precipitation undergoes evaporation during infiltration and recharge processes. The samples in this study were collected during summer, which is when precipitation in the study area is predominantly concentrated. Consequently, precipitation exerts the greatest influence on the other water bodies in study area; however, the stable isotopic signature of groundwater is more depleted than local precipitation (Fig. 8b). It may be attributable to various factors, including winter precipitation recharge, paleowater recharge formed by precipitation in a cooler climate since the late Pleistocene (Priestley et al. 2020; Zhao et al. 2012), and recharge from areas with more depleted precipitation δD and $\delta^{18}\text{O}$ compositions (Jasechko 2019). In the study area, precipitation is primarily concentrated in summer (Fig. 1d), and the isotopic signature of local precipitation depends on summer precipitation. Considering that groundwater represents a

mixture of precipitation over an extended period, the impact of winter precipitation on the groundwater isotopic signature is relatively restricted; hence, the deviation due to winter precipitation recharge does not appear to be a reasonable explanation. Tritium, with a half-life of 12.43 years, serves as one of the commonly utilized isotopes for assessing groundwater age (Terzer-Wassmuth et al. 2022). The high tritium values in groundwater and river water suggest that the groundwater in the study area is not palaeo-groundwater recharged during the cold period but rather a product of modern precipitation (after the nuclear explosion tests in the 1960s).

The stable isotopic signature of groundwater at the source of the Laoha River (SLH) and the source of the Xilamulun River (SXLML) are significantly variable (Fig. 8c). The mean values of stable isotopes of groundwater in SLH ($\delta D = -71.52\text{‰}$, $\delta^{18}O = -9.13\text{‰}$) are more enriched than those of SXLML ($\delta D = -87.02\text{‰}$, $\delta^{18}O = -11.14\text{‰}$). If infiltration of modern precipitation is the only way to recharge groundwater, then the distribution of groundwater δD and $\delta^{18}O$ composition should be broad and have no spatial variation. However, there are obvious differences in groundwater stable isotopes in different river sources, indicating spatial specificity in groundwater recharge.

Spatial specificity in groundwater recharge is commonly a result of geologic influences. The study area is located in the CAOB with widespread geological structural features. The discrepancy in δD – $\delta^{18}O$ composition between the local precipitation and groundwater, which is recharged from modern precipitation (post 1960s), is not unique to this study area. Similar phenomena exist in other areas where faults and volcanoes are developed (Abdelmohsen et al. 2019; Ma et al. 2022; Wang et al. 2017b). In these areas, faults and volcanoes are considered to play a crucial role in groundwater circulation. The $^3\text{He}/^4\text{He}$ ratio (R) is often used to trace groundwater circulation (Mahara and Igarashi 2003; Stute et al. 1992). Atmospheric contamination during sampling can be corrected using the $^4\text{He}/^{20}\text{Ne}$ ratio (see “Materials and methods” for details). If the R_c exceeds $0.1R_a$, it is considered to be clearly affected by mantle-derived helium (Hoke et al. 2000). As shown in Fig. 8e, all the air-corrected helium isotope ratios in groundwater exceed $0.1R_a$. The proportion of mantle-derived helium (PM) mixing in the samples was calculated from equation (3) to range from 13.1 to 45.6% (Table S1 in the ESM). All air-corrected helium isotope ratios increased, indicating that air-contamination reduced the helium ratio in the water bodies. Even though well water samples W6 and W5 provided uncorrected helium isotope ratios, it is reasonable to assume that all groundwater samples possess mantle-derived characteristics, as their uncorrected helium ratios already exceed R_a (Fig. 8d) and will increase after correction. Helium is an extremely fugitive gas. As it dissolves into river water, due to the exchange between the river and the atmosphere, the helium concentration between the two will quickly reach equilibrium, resulting in $R_m/R_a = 1$. Consequently, even without correction, their $R_m > R_a$ of river

samples is enough to indicate a clear mantle-derived helium input. Three of the four springs have helium isotope ratios of $0.1 < R_m/R_a < 1$, which is lower than the other samples. The TDS values of the springs ranged from 232 to 3400 mg/L, with samples showing low helium isotope ratios presenting higher TDS values. Therefore, it is inferred that their lower R/R_a value was a result of the longer crustal-derived helium contaminating the groundwater and diluting the ratio. The results indicate that the groundwater in the study area experiences a mixing of mantle- and crustal-derived helium. Mantle-derived helium in the shallow aquifer signifies the existence of a channel for upward migration of mantle fluids, possibly related to the frequent geological activities. Volcano-associated features and deep faults often serve as fast channels, facilitating the upward transport of mantle fluids (Wang et al. 2020).

Groundwater in Dalinor Lake basin, and the surrounding area, recharge by sources external to study area, and according to the tritium values, this recharge source is modern precipitation (post 1960s). This requires the existence of a preferential channel for concentrated recharge in the groundwater circulation mechanism. The study area is crossed by the EW-oriented ultra-crust the Xar Moron fault (Fig. 1b), which provides suitable conditions for upward fluid transport. The latest activity of the Dalinor volcanic group dates to Holocene and the possibility of future eruptions remains (Zhao et al. 2017), and the Dalinor basalt is thought to be formed by the asthenosphere material at 60–100 km depth, rising to the surface through tectonic fissures (e.g. Xar Moron fault; Ye et al. 2020). Combined with the mantle-derived helium in groundwater, it can be assumed that geological formations control groundwater circulation. Considering the aforementioned factors, a more plausible explanation is that modern precipitation (post 1960s) from outside the area recharges groundwater in Dalinor Lake and its surrounding area through preferential channels, particularly the fault system. The results show that the groundwater in the study area exhibits depleted stable isotopes, high tritium values and rapid transport through geological formations. Hence, prospective recharge source areas should encompass (1) rivers or lakes seeping through topographical structure, (2) water bodies exhibiting depleted stable isotopic signatures and high tritium values, and (3) elevations higher than the study area. Owing to the constraints of the study, the specific recharge source areas require additional exploration in future studies.

Conclusions

Water resources are being lost in the Inner Mongolia plateau. The dataset obtained based on Landsat information shows that Dalinor Lake area had decreased 12% between 1986 and 2021, with an overall decreasing trend. Since 2005, the decrease rate of lake area has increased from -0.31 to -1.24

km²/year, a four-fold increase. The water balance results show that the contribution of groundwater to Dalinor Lake can reach 1.49×10^8 m³/year. Groundwater accounts for 62.5% of the annual recharge of the lake. The soil profiles and the rainfall simulation test conducted in the sandy area indicate that precipitation finds it difficult to infiltrate and recharge groundwater. The stable isotopes of groundwater samples from Dalinor Lake and its surrounding areas are more depleted than local precipitation, indicating that groundwater is not mainly recharged by local precipitation. Groundwater recharge is spatially specific, resulting in differences in stable isotopes of groundwater at different river sources. High tritium concentrations in groundwater and river water samples suggest a modern source of groundwater recharge. Combined with the mantle-derived helium found in groundwater and river water, it is speculated that groundwater in the study area receives recharge from modern precipitation (post 1960s). The modern precipitation with depleted stable isotope composition derived from outside the study area contributes to the groundwater through fast channels such as volcano-associated features or faults. This result demonstrates the role of geological structure in controlling the groundwater circulation in and around Dalinor Lake, which should be considered in water-resource-management strategies.

Supplementary information The online version contains supplementary material available at <https://doi.org/10.1007/s10040-023-02684-9>.

Acknowledgements We are grateful for the help of the State Key Laboratory of Hydrology–Water Resources and Hydraulic Engineering at Hohai University.

Funding This work was supported by the National Natural Science Foundation of China (No. 61771183).

Declarations

Conflict of interest The authors declare that they have no conflict of interest

References

- Abdelmohsen K, Sultan M, Ahmed M, Save H, Elkaliouby B, Emil M, Yan E, Abotalib AZ, Krishnamurthy RV, Abdelmalik K (2019) Response of deep aquifers to climate variability. *Sci Total Environ* 677:530–544. <https://doi.org/10.1016/j.scitotenv.2019.04.316>
- Bai M, Mo X, Liu S, Hu S (2020) Detection and attribution of lake water loss in the semi-arid Mongolian plateau: a case study in the Lake Dalinor. *Ecohydrology*. <https://doi.org/10.1002/eco.2251>
- Ballentine CJ, Burnard PG (2002) Production, release and transport of noble gases in the continental crust. *Rev Mineral Geochem* 47(1):481–538. <https://doi.org/10.2138/rmg.2002.47.12>
- Bowen GJ, Putman A, Brooks JR, Bowling DR, Oerter EJ, Good S (2018) Inferring the source of evaporated waters using stable H and O isotopes 187:1025–1039. <https://doi.org/10.1007/s00442-018-4192-5>
- Bureau of Hydrology, Ministry of Water Resources, P R.China (2006–2011) Hydrological data of liaohe river basin in annual hydrological report P. R. China [M] Beijing: Bureau of Hydrology, Ministry of Water Resources
- CAS (2015) Geospatial Data Cloud. Computer Network Information Center, Chinese Academy of Sciences. <http://www.gscloud.cn/>. Accessed 1 December 2021
- Dai GS, Ulgiati S, Zhang YS, Yu BH, Kang MY, Jin Y, Dong XB, Zhang XS (2014) The false promises of coal exploitation: how mining affects herdsman well-being in the grassland ecosystems of Inner Mongolia. *Ener Pol* 67:146–153. <https://doi.org/10.1016/j.enpol.2013.12.033>
- Dekker LW, Ritsema CJ (1996) Preferential flow paths in a water repellent clay soil with grass cover. *Water Resour Res* 32:1239–1249. <https://doi.org/10.1029/96wr00267>
- Dogramaci S, Skrzypek G, Dodson W, Grierson PF (2012) Stable isotope and hydrochemical evolution of groundwater in the semi-arid Hamersley Basin of subtropical Northwest Australia. *J Hydrol* 475:281–293. <https://doi.org/10.1016/j.jhydrol.2012.10.004>
- Dong X, Chen Z, Wu M, Hu C (2020) Long time series of remote sensing to monitor the transformation research of Kubuqi Desert in China. *Earth Sci Inform* 13:795–809. <https://doi.org/10.1007/s12145-020-00467-4>
- Du Z, Zhao J, Cheng J (1997) Unsaturated seepage test in loess (in Chinese). *Hydrogeol Eng Geol* 02:50–52
- Du L, Li C, Li W, Shi X (2019) Spatial variation characteristics of composition of hydrogen and oxygen stable isotopes in water of Dalinor Lake and their influencing factors (in Chinese). *Wetl Sci* 17:216–221. <https://doi.org/10.13248/j.cnki.wetlandsci.2019.02.013>
- Gardner WR (1960) Dynamic aspects of water availability to plants. *Soil Sci* 89:63–73. <https://doi.org/10.1097/00010694-19602000-00001>
- Ge J, Chen J, Ge L, Wang T, Wang C, Che Y (2016) Isotopic and hydrochemical evidence of groundwater recharge in the Hopq Desert, NW China. *J Radioanal Nucl Chem* 310:761–775. <https://doi.org/10.1007/s10967-016-4856-8>
- Goldberg D, Gornat B, Rimon D (1976) Drip irrigation: principles, design and agricultural practices. *J Water Resour Protect* 11(9)
- Gong L, Li N, Fan Q, Zhao Y, Zhang L, Zhang C (2016) Mapping the topography and cone morphology of the Dalinor volcanic swarm in Inner Mongolia with remote sensing and DEM data. *Front Earth Sci* 10:578–594. <https://doi.org/10.1007/s11707-015-0536-1>
- Graham DW (2002) Noble gas isotope geochemistry of Mid-Ocean ridge and Ocean Island basalts: characterization of mantle source reservoirs. *Rev Mineral Geochem* 47:247–317. <https://doi.org/10.2138/rmg.2002.47.8>
- Guo X, Feng Q, Si J, Xi H, Zhao Y, Deo C (2019) Partitioning groundwater recharge sources in multiple aquifers system within a desert oasis environment: implications for water resources management in endorheic basins. *J Hydrol* 579:124212. <https://doi.org/10.1016/j.jhydrol.2019.124212>
- Hilton DR (1996) The helium and carbon isotope systematics of a continental geothermal system: results from monitoring studies at Long Valley caldera (California, U.S.A.). *Chem Geol* 127:269–295. [https://doi.org/10.1016/0009-2541\(95\)00134-4](https://doi.org/10.1016/0009-2541(95)00134-4)
- Hoke L, Lamb S, Hilton DR, Poreda RJ (2000) Southern limit of mantle-derived geothermal helium emissions in Tibet: implications for lithospheric structure. *Earth Planet Sci Lett* 180:297–308. [https://doi.org/10.1016/S0012-821X\(00\)00174-6](https://doi.org/10.1016/S0012-821X(00)00174-6)
- Huang X, Jiang D, Dong X, Yang S, Su B, Li X, Tang Z, Wang Y (2019) Northwestward migration of the northern edge of the east Asian summer monsoon during the mid-Pliocene warm period: simulations and reconstructions. *J Geophys Res: Atmos* 124:1392–1404. <https://doi.org/10.1029/2018jd028995>

- Jasechko S (2019) Global isotope hydrogeology: review. *Rev Geophys* 57:835–965. <https://doi.org/10.1029/2018rg000627>
- Li D, Tian P, Luo Y, Dong B, Cui Y, Khan S (2021) Importance of stopping groundwater irrigation for balancing agriculture and wetland ecosystem. *Ecol Indic* 127:107747. <https://doi.org/10.1016/j.ecolind.2021.107747>
- Li W, Liu Z, Yang X, Li C (2019) Changes of stable oxygen and hydrogen isotopes in the summer at Dalinor Lake in Inner Mongolia of northern China (in Chinese). *J Lake Sci* 31:539–550
- Li W, Wang L, Zhang Y, Wu L, Zeng L, Tuo Z (2021) Determining the boundary of groundwater basin of Dalinuoer Lake watershed in the middle of inner Mongolian plateau, China and its impact on the ecological environment, China. *Geology* 4:1–11. <https://doi.org/10.31035/cg2021066>
- Li Z, Chen X, Liu W, Si B (2017) Determination of groundwater recharge mechanism in the deep loessial unsaturated zone by environmental tracers. *Sci Total Environ* 586:827–835. <https://doi.org/10.1016/j.scitotenv.2017.02.061>
- Liu J, Song X, Yuan G, Sun X, Yang L (2014) Stable isotopic compositions of precipitation in China. *Tellus B: Chem Phys Meteorol* 66:22567. <https://doi.org/10.3402/tellusb.v66.22567>
- Lozowski EP, Charlton RB, Nguyen CD, Wilson JD (1989) The use of cumulative monthly mean temperature anomalies in the analysis of local interannual climate variability. *J Clim* 2:1059–1068. [https://doi.org/10.1175/1520-0442\(1989\)002<1059:TUOCM M>2.0.CO;2](https://doi.org/10.1175/1520-0442(1989)002<1059:TUOCM M>2.0.CO;2)
- Ma F, Chen J, Chen J, Wang T (2022) Hydrogeochemical and isotopic evidences of unique groundwater recharge patterns in the Mongolian plateau. *Hydrol Process* 36(5):e14554. <https://doi.org/10.1002/hyp.14554>
- Ma Y, Zhao J, Luo X, Shao T, Yue D, Zhao Q (2016) Runoff and groundwater recharge conditions in the megadune area of Badain Jaran Desert. *Acta Geograph Sin* 71:433–448. <https://doi.org/10.11821/dlxb201603007>
- Mahara Y, Lgarashi T (2003) Changes in isotope ratio and content of dissolved helium through groundwater evolution. *Appl Geochem* 18:719–738. [https://doi.org/10.1016/S0883-2927\(02\)00177-4](https://doi.org/10.1016/S0883-2927(02)00177-4)
- Marty B, Le Cloarec MF (1992) Helium-3 and CO₂ fluxes from bacterial volcanoes estimated from polonium-210 emissions. *J Volcanol Geotherm Res* 53:67–72. [https://doi.org/10.1016/0377-0273\(92\)90074-N](https://doi.org/10.1016/0377-0273(92)90074-N)
- Mu H, Chen H, Zhang Z, Zhang B (2021) National spatial database of 1:200 000 regional hydrogeological maps, China. *Geology* 48:124–138. <https://doi.org/10.12029/gc2021Z212>
- Niu J, Yu X, Zhang Z (2006) The present and future research on preferential flow (in Chinese). *Acta Ecol Sin* 26:231–243
- Ozima M, Podosek FA (2002) Noble gas geochemistry. Cambridge University Press, New York
- Pekel JF, Cottam A, Gorelick N, Belward AS (2016) High-resolution mapping of global surface water and its long-term changes. *Nature* 540:418–422. <https://doi.org/10.1038/nature20584>
- Priestley SC, Meredith KT, Treble PC, Cendon DI, Griffiths AD, Hollins SE, Baker A, Pigois JP (2020) A 35 ka record of groundwater recharge in South-West Australia using stable water isotopes. *Sci Total Environ* 717:135105. <https://doi.org/10.1016/j.scitotenv.2019.135105>
- Qin Z, Peng TS, Vijay P, Chen M (2019) Spatio-temporal variations of precipitation extremes in Hanjiang River basin, China, during 1960–2015. *Theor Appl Climatol* 138:1767–1783. <https://doi.org/10.1007/s00704-019-02932-7>
- Ren T, Zhao Q, Chen B, Gao P, Chen J, Deng G, Kuang Y, Liu Y, Wang W, Liu Z (2005) Tritium concentrations of surface and underground waters in China (in Chinese). *Chin J Radiol Med Protection* 25:466–472
- Ren X, Zhu B, Liu M, Zhang Y, He Z, Rioual P (2018) Mechanism of groundwater recharge in the middle-latitude desert of eastern Hunshandake, China: diffuse or focused recharge? *Hydrogeol J* 27:761–783. <https://doi.org/10.1007/s10040-018-1880-5>
- SEPA (2001) China's second national report on implementation of the convention on biological diversity. China Environmental Science Press, Beijing
- Shen Z, Zhang Q, Chen D, Singh VP (2021a) Varying effects of mining development on ecological conditions and groundwater storage in dry region in Inner Mongolia of China. *J Hydrol* 597:125759. <https://doi.org/10.1016/j.jhydrol.2020.125759>
- Shen Z, Zhang Q, Piao S, Peñuelas J, Stenseth NC, Chen D, Xu CY, Singh VP, Liu T (2021b) Mining can exacerbate global degradation of dryland. *Geophys Res Lett* 48:e2021GL094490. <https://doi.org/10.1029/2021GL094490>
- Shurbaji ARM, Phillips FM, Campbell AR, Knowlton RG (1995) Application of a numerical model for simulating water flow, isotope transport, and heat transfer in the unsaturated zone. *J Hydrol* 171:143–163. [https://doi.org/10.1016/0022-1694\(95\)02756-F](https://doi.org/10.1016/0022-1694(95)02756-F)
- Stute M, Sonntag C, Déak J, Schlosser P (1992) Helium in deep circulating groundwater in the great Hungarian plain: flow dynamics and crustal and mantle helium fluxes. *Geochim Cosmochim Acta* 56:2051–2067. [https://doi.org/10.1016/0016-7037\(92\)90329-H](https://doi.org/10.1016/0016-7037(92)90329-H)
- Terzer-Wassmuth S, Araguas-Araguas LJ, Copia L, Wassenaar LI (2022) High spatial resolution prediction of tritium (3H) in contemporary global precipitation. *Sci Rep* 12:10271
- USGS (2011) The USGS global visualization viewer. <http://glovis.usgs.gov/>. Accessed 1 December 2021
- Wang T, Chen J, Xu Y, Zhan L, Huang D (2017a) Isotopes and hydrochemistry of Daihai Lake recharging sources, northern China. *J Radioanal Nucl Chem* 312:615–629. <https://doi.org/10.1007/s10967-017-5241-y>
- Wang X, Hou X, Wang Y (2017b) Spatiotemporal variations and regional differences of extreme precipitation events in the coastal area of China from 1961 to 2014. *Atmos Res* 197:94–104. <https://doi.org/10.1016/j.atmosres.2017.06.022>
- Wang X, Li X, Kang E, Zhang J, Zhou H, Yang S, Lei Z (2003) The infiltration and redistribution of precipitation in revegetated sand dunes in the Tengger Desert, Shapotou, China (in Chinese). *Acta Ecol Sin* 23:1235–1241
- Wang Y, Liu Y, Zhao C, Li Q, Zhou Y, Ran H (2020) Helium and carbon isotopic signatures of thermal spring gases in Southeast Yunnan, China. *J Volcanol Geotherm Res* 402:106995. <https://doi.org/10.1016/j.jvolgeores.2020.106995>
- Weiss RF (1971) Solubility of helium and neon in water and seawater. *J Chem Eng Data* 16:235–241. <https://doi.org/10.1021/jc60049a019>
- Wu Y, Liu T, Paredes P, Duan L, Wang H, Wang T, Pereira LS (2016) Ecohydrology of groundwater-dependent grasslands of the semi-arid Horqin sandy land of Inner Mongolia focusing on evapotranspiration partition. *Ecohydrology* 9:1052–1067. <https://doi.org/10.1002/eco.1702>
- Xing Z, Huang H, Li Y, Liu S, Wang D, Yuan Y, Zhao Z, Bu L (2021) Management of sustainable ecological water levels of endorheic salt lakes in the inner Mongolian plateau of China based on eco-hydrological processes. *Hydrol Process* 35(5):e14192. <https://doi.org/10.1002/hyp.14192>
- Xu Y, Gun Z, Zhao J, Cheng X (2022) Variations in lake water storage over Inner Mongolia during recent three decades based on multi-mission satellites. *J Hydrol* 609:127719. <https://doi.org/10.1016/j.jhydrol.2022.127719>
- Yang H, Liu J, Liang H (2009) Change characteristics of climate and water resources in west Liaohé River plain (in Chinese). *J Appl Ecol* 20:84–90
- Yang X, Scuderi LA, Wang X, Scuderi LJ, Zhang D, Li H, Forman S, Xu Q, Wang R, Huang W, Yang S (2015) Groundwater sapping as the cause of irreversible desertification of Hunshandake Sandy lands, Inner Mongolia, northern China. *Proc Natl Acad Sci USA* 112:702–706. <https://doi.org/10.1073/pnas.1418090112>

- Ye G, Fu H, Jin S, Wei W (2020) Magnetotelluric study of the mechanism of the Abaga and Dalinor volcanic groups in Central Inner Mongolia, China. *Phys Earth Planet Inter* 308:106570. <https://doi.org/10.1016/j.pepi.2020.106570>
- Yin Z, Xu Y, Zhu X, Zhao J, Yang Y, Li J (2021) Variations of groundwater storage in different basins of China over recent decades. *J Hydrol* 598:126282. <https://doi.org/10.1016/j.jhydrol.2021.126282>
- Yu X, Wu Y, Jiang C, Zhang Z, Du X, Liu T (2020) Magnetic resonance sounding evidence shows that shallow groundwater discharge maintains the lake landscape in the Hunshandake Sandy land, North China. *Environ Earth Sci* 79:327. <https://doi.org/10.1007/s12665-020-09076-2>
- Zhang M, Wang S (2016) A review of precipitation isotope studies in China: basic pattern and hydrological process. *J Geogr Sci* 26:921–938. <https://doi.org/10.1007/s11442-016-1307-y>
- Zhang S, Gao R, Li H, Hou H, Wu H, Li Q, Yang K, Li C, Li W, Zhang J, Yang T, Keller GR, Liu M (2014) Crustal structures revealed from a deep seismic reflection profile across the Solonker suture zone of the central Asian Orogenic Belt, northern China: an integrated interpretation. *Tectonophysics* 612–613:26–39. <https://doi.org/10.1016/j.tecto.2013.11.035>
- Zhang Y, Wei Y, Liao Z, Xu X, Han Z, Liang W, Long Y, Guo J (2020) Determination of soil-groundwater systems recharge mechanism in the middle Inner Mongolia plateau by isotopic tracers. *Environ Earth Sci* 79:473. <https://doi.org/10.1007/s12665-020-09226-6>
- Zhang Z, Lu Y, Wu G, Wang Y (2017) Retrieval of precipitation for grassland based on the multi-temporal Sentinel-1 SAR data (in Chinese). *Rem Sensing Nat Resour* 29:156–160
- Zhao L, Xiao H, Dong Z, Xiao S, Zhou M, Cheng G, Yin L, Yin Z (2012) Origins of groundwater inferred from isotopic patterns of the Badain Jaran Desert, northwestern China. *Ground Water* 50:715–725. <https://doi.org/10.1111/j.1745-6584.2011.00895.x>
- Zhao Y, Fan Q, Li N, Gong L (2017) Study on volcanic geology characteristics and magma feeding fractures of Late Quaternary volcanoes in Dalinor volcanic field, Inner Mongolia. *Acta Petrol Sin* 33:127–136. <https://doi.org/10.1371/journal.pone.0221177>
- Zhao Z, Lin A, Feng J, Yang Q, Zou L (2016) Analysis of water resources in Horqin Sandy land using multisource data from 2003 to 2010. *Sustainability* 8(4):374–391. <https://doi.org/10.3390/su8040374>
- Zhen Z, Li C, Li W, Hu Q, Liu X, Liu Z, Yu R (2014) Characteristics of environmental isotopes of surface water and groundwater and their recharge relationships in Lake Dali basin. *J Lake Sci* 26:916–922
- Zhen Z, Li W, Xu L, Zhang X, Zhang J (2021) Lake-level variation of Dali Lake in mid-east of inner Mongolia since the Late Holocene. *Quat Int* 583:62–69. <https://doi.org/10.1016/j.quaint.2021.03.003>
- Zheng J, Ke C, Shao Z, Li F (2016) Monitoring changes in the water volume of Hulun Lake by integrating satellite altimetry data and Landsat images between 1992 and 2010. *J Appl Remote Sens* 10(1):016029. <https://doi.org/10.1117/1.Jrs.10.016029>
- Zheng Y, Liu H, Zhuo Y, Li Z, Liang C, Wang L (2019) Dynamic changes and driving factors of wetlands in Inner Mongolia plateau, China. *PLoS One* 14:e0221177
- Zhu BQ, Ren XZ, Rioual P (2019) Geological control on the origin of fresh groundwater in the Otindag Desert, China. *Appl Geochem* 103:131–142. <https://doi.org/10.1016/j.apgeochem.2019.03.006>

Publisher's note Springer Nature remains neutral with regard to jurisdictional claims in published maps and institutional affiliations.

Springer Nature or its licensor (e.g. a society or other partner) holds exclusive rights to this article under a publishing agreement with the author(s) or other rightsholder(s); author self-archiving of the accepted manuscript version of this article is solely governed by the terms of such publishing agreement and applicable law.